Absence of static magnetic order in nonsuperconducting FeSe thin films on SrTiO$_3$(001) revealed by the magnetism of Se vacancies

Weijiong Chen,[1] Zijun Tian,[1] Ping Li,[1] Weidong Luo,[1,3,4,*] and C. L. Gao[2,4,†]

[1]*Key Laboratory of Artificial Structures and Quantum Control, School of Physics and Astronomy, Shanghai Jiao Tong University, Shanghai 200240, China*

[2]*State Key Laboratory of Surface Physics and Department of Physics, Fudan University, Shanghai 200433, China*

[3]*Institute of Natural Sciences, Shanghai Jiao Tong University, Shanghai 200240, China*

[4]*Collaborative Innovation Center of Advanced Microstructures, Nanjing 210093, China*

FeSe, as the simplest Fe-based superconductor, invokes tremendous studies on its electronic and magnetic properties. Among these, inconsistent or even contradictory results are often seen in both theory and experiment, especially concerning the magnetism of FeSe. In this paper, the absence of static magnetic order is directly revealed by the magnetism of Se vacancies in FeSe thin films on SrTiO$_3$ measured with spin-polarized scanning tunneling microscopy on the atomic scale. Symmetry analysis and first-principles calculation further confirmed the nonmagnetic ground state of FeSe. The discrepancy between local-density approximation and generalized-gradient approximation implies that FeSe is near a magnetic critical point.

The Fe-based superconductor has gained intensive interest ever since its discovery in 2008 [1]. Among various Fe pnictides and Fe chalcogenides, the stoichiometric FeSe draws particular attention because it has the simplest crystal structure, yet possesses rich structural, electronic, and magnetic properties in both bulk crystal and thin films [2]. Bulk FeSe has a superconducting transition temperature (T_c) of 8 K [1] which can be raised to 37 K [3,4] coexisting with a static magnetic order under high pressure [5,6]. FeSe films can be grown on different substrates [7–9]. On graphene, FeSe films show similar superconductivity to the bulk crystal with a thickness dependence of T_c [8]. However, unexpected superconductivity was discovered in single layer FeSe on SrTiO$_3$(001) [7] with T_c up to over 100 K [10]. Surprisingly, starting from 2 layers, FeSe thin films grown on SrTiO$_3$(001) do not show any superconductivity owing to tensile force induced by lattice mismatch between FeSe and SrTiO$_3$ as well as on MgO and LaAlO$_3$ [9,11]. Furthermore, the superconductivity of FeSe thin films can be restored and further enhanced by surface electron doping of potassium [12–15] which implies that not only the lattice constant but also the electron doping effect has a great influence on the properties of FeSe.

Both theoretical and experimental efforts have been made to study the magnetic properties of FeSe. In contradiction to most early theoretical predictions of antiferromagnetic (AFM) order [16–18], bulk FeSe does not display any AFM order under ambient pressure. Recently, it was theoretically proved that the missing AFM order might be caused by magnetic frustration [19–21] and, then, be substituted by so-called nematic quantum paramagnetic phase [22–24]. However, this is not conclusive for FeSe thin films due to the stress caused by lattice mismatch and the difficulty in measuring the magnetism in the thin-film limit. Early angle-resolved photoemission spectroscopy (ARPES) study on 3–50-layer FeSe on SrTiO$_3$ suggested that an electronic structure renormalization took place at low temperature with the emergence of spin-density wave (SDW) phase as the superconductivity was suppressed [11], which was later found in bulk FeSe as well [25–28] and was attributed to the nematic phase instead. The most magnetic relevant measurement was done recently by an indirect measurement through the magnetic exchange bias effect of FeNi on FeSe where the FeSe film was claimed as antiferromagnetic while the bulk FeSe as nonmagnetic [29].

In this paper, to resolve the discrepancy concerning the magnetism of FeSe thin film, we report a direct measurement of the magnetic properties of FeSe thin film grown on SrTiO$_3$(001) utilizing spin-polarized scanning tunneling microscopy (SPSTM). Unlike the isostructural FeTe which possesses a bicollinear antiferromagnetic order as observed by SPSTM [30], FeSe does not show any antiferromagnetic superstructure. A paramagnetic behavior of isolated Se vacancies was found indicating that FeSe film is nonmagnetic which was further confirmed by combining the symmetry analysis and first-principles calculation.

FeSe thin film was grown on 0.7% Nb-doped SrTiO$_3$(001) by molecular-beam epitaxy in ultrahigh vacuum (1×10^{-10} mbar). The SrTiO$_3$ substrate was prepared by annealing at $1000\,^\circ$C for 1 h in vacuum and kept at $400\,^\circ$C during film growth. High-purity Fe (99.995%) and Se (99.999%) were coevaporated onto the substrate with Se/Fe flux ratio of $\sim$10. The growth process was monitored by reflective high-energy electron diffraction (RHEED). SPSTM measurements were done at 4.2 K in a vector magnetic field. The magnetic tips were prepared by coating antiferromagnetic Cr on flashed tungsten tips. The scanning tunneling spectroscopy (STS) was obtained using the lock-in technique with a 4-mV modulation at 985 Hz. Details of SPSTM can be found eleswhere [31].

First-principles calculation are used to explain the experimental data. All electronic structure calculations were carried out by using the density-functional theory and the projector augmented-wave (PAW) method [32,33], which is implemented in the VASP code [34,35]. Both the local-density approximation (LDA) [36] and the generalized-gradient approximation (GGA) [37] were adopted. We constructed a

---

*Corresponding author: wdluo@sjtu.edu.cn

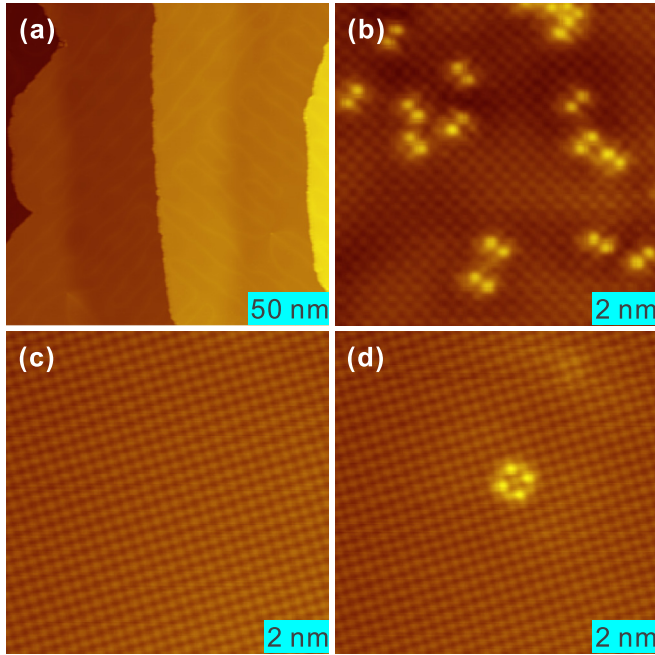†Corresponding author: clgao@fudan.edu.cn

FIG. 1. STM image of FeSe thin film grown on $SrTiO_3$: (a) Topography image of approximately 20-layer FeSe films on $SrTiO_3(001)$ ($U = -138$ mV, $I = 100$ pA, 200 nm×200 nm). Atomic resolved images of (b) the as-grown sample ($U = 100$ mV, $I = 100$ pA, 10 nm×10 nm), (c) the sample after annealing at $440\,°C$ for 10 h ($U = -100$ mV, $I = 300$ pA, 10 nm×10 nm), and (d) an isolated Se vacancy on annealed sample surface ($U = -100$ mV, $I = 300$ pA, 10 nm×10 nm).

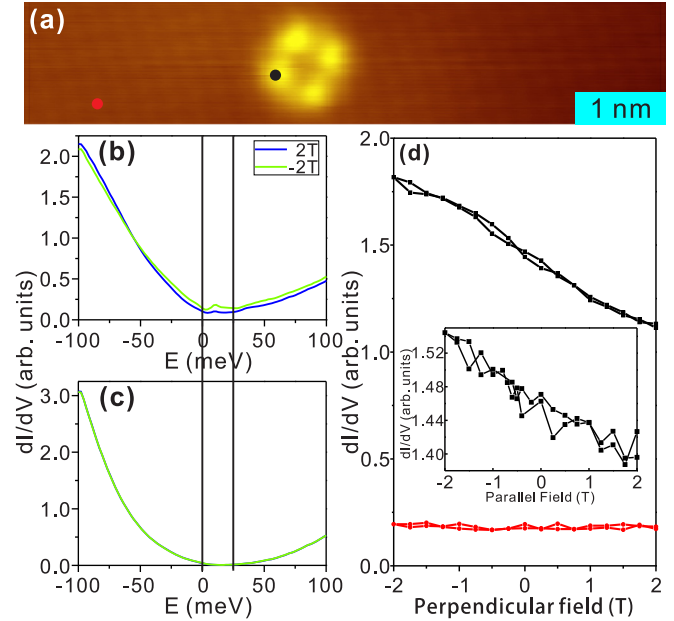

FIG. 2. Spin-polarized scanning tunneling spectroscopy on VNN Se site and VFA Se site: (a) Topography of an isolated Se vacancy in FeSe films ($U = -100$ mV, $I = 800$ pA) (b) [(c)] STS curves measured with an antiferromagnetic Cr-tip at the black [red] dot in (a) under the perpendicular magnetic field of 2 T (blue curves) and -2 T (green curves). (d) The magnetic loops measured with the same Cr tip at the black dot (black curves) and the red dot (red curves) in (a) illustrating the average of the dI/dV value between 0 and 25 meV [the region is printed in (b) and (c) by black lines] vs the perpendicular magnetic fields [inset in (d) vs the parallel magnetic fields].

$4\sqrt{2} \times 4\sqrt{2}$ supercell with the Se vacancy at the center of it to simulate the experiment and a $\sqrt{2} \times \sqrt{2}$ supercell for perfect FeSe with different magnetic orders. The plane-wave cutoff energy was chosen to be 286 eV, and a Γ mesh of $16 \times 16 \times 1$ k points and 1 Γ point were used for the perfect FeSe and the supercell with the vacancy. To decouple the neighboring FeSe layers, a vacuum layer over 20 Å thick was used in the calculation. The atomic positions were fully optimized in all the magnetic orders until the atomic forces were smaller than 0.01 eV/Å, but both the lattice constant a and b were set to 3.77 Å and remained unchanged throughout the calculation.

Figure 1(a) gives the overall morphology of about 20 layers FeSe. The surface is atomically flat with terraces around 100 nm in width. The stripe-shaped corrugations on the surface result from the tensile strain of film-substrate lattice mismatch [38]. The as-grown film contains many bright dumbbell-like pairs on the surface, as shown in the atomically resolved image in Fig. 1(b), which are believed to be Fe vacancies caused by excess Se [39]. The existence of a large amount of Fe vacancies can dramatically change the electronic structure of FeSe film and even transform the metallic FeSe film into a semiconductor/insulator with $\sqrt{5} \times \sqrt{5}$ Fe vacancy order [40]. A similar process was also reported to happen in superconducting FeSe on graphene, where the superconductivity is spoiled with just over 2.5% of Fe vacancies [8]. These Se-rich defects can be fully removed by annealing the film at $440\,°C$ for about 10 h. The defect-free squarelike lattice as shown in Fig. 1(c) indicates the high

quality of FeSe thin film. Each bright spot in the STM image corresponds to a Se atom above the Fe plane. As in the previous study [7,38], superconductivity is not found in our sample. The suppression of superconductivity is thought to result from the tensile strain caused by $SrTiO_3$ substrate [9]. In some area, an isolated defect was observed [Fig. 1(d)] which appears as four bright spots in fourfold symmetry. Considering the crystal structure, the center of the defect is at the Se site which is located at the fourfold rotation axis, while an iron atom is located at the twofold rotation axis. Therefore, we believe this kind of defect is caused by one missing Se atom through overannealing, which induces the change of local density of states (LDOS) of the four neighboring Se atoms. The Se vacancies with similar topography are also found in bulk cleaved FeSe [41] and superconducting FeSe film grown on graphene [8]. However, further long-time annealing (up to 20 h) does not dramatically change the density of Se vacancies after the density reaches about 1–2 vacancies per 900 nm^2.

The magnetic property of the FeSe surface was measured with antiferromagnetic Cr tips. First of all, unlike the obvious antiferromagnetic superstructure observed by SPSTM in a similar system, FeTe [30], there is not any trace of magnetic superstructure in the SPSTM images on FeSe. Magnetic contrast, however, was observed on Se vacancies. Figures 2(b) and 2(c) give dI/dV spectroscopies taken by the same Cr tip under opposite external perpendicular magnetic field on the Se vacancy and defect-free surface, respectively. It can

(a) 0.5 T

(b) -0.5T

(c) Subtraction
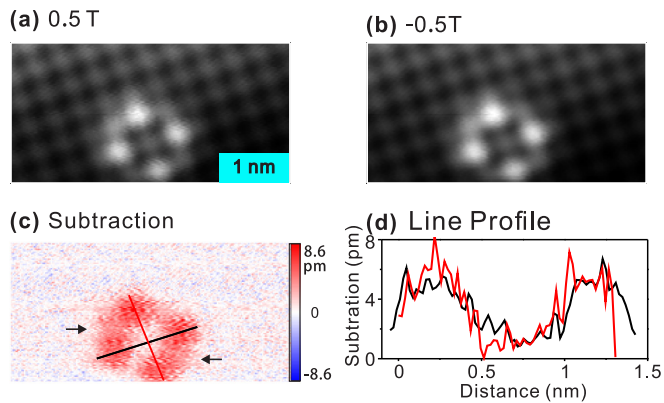

(d) Line Profile

FIG. 3. The spatial distribution of magnetic contrast near the Se vacancy: Thermal-drift corrected STM topography of an isolated Se vacancy in FeSe films scanned under the opposite perpendicular magnetic fields 0.5 T (a) and -0.5 T (b) with the same antiferromagnetic Cr tip and the same parameter ($U = -100$ mV, $I = 500$ pA). (c) The subtraction image of (a) and (b). (d) The line profiles across the defect in (c).

be seen in Fig. 2(b) that the two curves, which were taken on one of the four bright spots around Se vacancy [vacancy-nearest-neighbor (VNN) Se site] as marked by the black dot in Fig. 2(a) under ± 2 T, do not coincide with each other. Since the antiferromagnetic Cr tip does maintain its magnetic orientation under external magnetic field, the change in the dI/dV curves must come from magnetic response of Se, i.e., the Se atom possesses a net spin polarization which changes with external field. On the other hand, on the Se atom far away from the defects [vacancy-far-away (VFA) Se site], the two curves totally overlap showing that these places are nonmagnetic [Fig. 2(c)].

To further clarify the magnetic properties of the Se vacancy, Fig. 2(d) plots the magnetic hysteresis loops of the Se defect as well as the bare surface. These loops were taken by averaging the dI/dV values between 0 and 25 meV [marked in Figs. 2(b) and 2(c)] versus the applied external field. At the VNN Se site, the magnetic loop displays a clear paramagnetic behavior under perpendicular magnetic field [the black curve in Fig. 2(d)] as well as under parallel magnetic field [the inset in Fig. 2(d)], while, at the VFA Se site, the dI/dV value does not show any change with the ramp of the external magnetic field [the red curve in Fig. 2(d)]. Considering that what SPSTM measures is the change of the relative spin-polarized direction of tip and the sample rather than pure magnetization of the sample, the negative field dependence of the spin-resolved dI/dV signal in Fig. 2(d) (negative slope) means the spin polarizations of the fixed tip and the alterable sample at that energy range become more antiparallel with increasing field. From the fact that the magnetization of the Se vacancy follows perfectly with the applied magnetic field, it can be concluded that FeSe thin film is nonmagnetic because otherwise the magnetization of the Se vacancy would be pinned by the magnetization of the film.

Further evidence of nonmagnetic FeSe thin film is conceived in the spatial distribution of the spin polarization around the Se vacancy. Figures 3(a) and 3(b) give the constant current images taken at opposite magnetic field ± 0.5 T. By subtracting Fig. 3(a) from Fig. 3(b), the topographic information was

eliminated and a net spin distribution was obtained as shown in Fig. 3(c). According to STS data shown in Fig. 2, there is no magnetization at the defect-free surface which is set as zero (white color) in Fig. 3(c), thus the red and blue color represent spin polarization of opposite directions. It can be seen clearly that the four VNN Se sites manifest nearly the same spin polarization which is shown in the line profiles [Fig. 3(d)] across the defects as well. From a symmetry point of view, the presence of any magnetic superstructure in the Fe layer will break the fourfold symmetry on the VNN Se sites in the spin channel (it will be discussed in detail later). Thus, the FeSe films must be nonmagnetic and the magnetization damps rapidly with the distance from the vacancy.

Previous theoretical and experimental studies have shown the complexity of the magnetic properties of FeSe. For the calculation, generally, GGA gives a collinear AFM (CAFM) structure as the ground state while LDA shows that the nonmagnetic state has the lowest energy. GGA and LDA are slightly different in optimizing the structure as well as in treating the electron interaction. This strong method's dependency suggests the calculated results are very sensitive to structural and computational details. The experimental results also show the complexities, especially in the thin films. Electronic reconstruction at low temperature associated with SDW is observed by ARPES measurement in FeSe films on SrTiO₃ [11], while exchange bias measurement suggests that antiferromagnetism exists in as-grown single layer FeSe on SrTiO₃ and is replaced by superconductivity after annealing [29]. Recently, a topological edge state was observed in single layer superconducting FeSe on SrTiO₃, which can be explained by the checkerboard AFM order including the spin orbital coupling effect [42]. All these complex, even contradictory, results in both theory and experiment strongly suggest that FeSe is very near a magnetic critical point. A slight difference in structure, stoichiometry, or Fermi level changes its magnetic property.

Consistent with the literature, we also found that LDA gives a nonmagnetic state while GGA gives CAFM as the most stable states. Apparently, although the optimized structure parameter (the Se height) from GGA agrees better with experiments, the magnetic properties from LDA agree better with our experiment. This result can be understood from the following two properties of DFT. First, as DFT is a mean-field theory, it underestimates the effect of spin fluctuations which generally suppress long-range magnetic order. Second, the gradient correction in GGA, compared to LDA, usually enhances local magnetic moments. Thus for systems with weak magnetism and when spin fluctuations play important roles, such as in FeSe, LDA better describes magnetic properties than GGA. This is similar to the situation in the iron pnictides [43,44]. Since it has been shown that FeSe is very near the magnetic critical point, in the following discussion of Se vacancy, we use GGA to optimize the Se height and then use LDA to calculate the magnetism.

First, the magnetic moments around the Se vacancy of nonmagnetic FeSe were calculated as shown in Fig. 4(a). The magnetic moments of Fe atoms form a radial oscillating decaying behavior away from the Se vacancy with the central four Fe atoms each possessing a magnetic moment as large as $1.68\mu_B$ pointing to the same direction. This staggered ferrimagnetic structure near the Se vacancy was also predicted

(a) ●Fe ●Top Se ●Bottom Se   **(b)**

```
-0.020  -0.006   0.290   0.290  -0.006  -0.020
   0.001   0.002   0.003   0.002   0.001
-0.006   0.099  -0.609  -0.609   0.099  -0.006
   0.002  -0.010  -0.013  -0.010   0.002
 0.290  -0.609   1.682   1.682  -0.609   0.290
   0.003          -0.013  -0.013          0.003
 0.290  -0.609   1.682   1.682  -0.609   0.290
   0.002  -0.010  -0.013  -0.010   0.002
-0.006   0.099  -0.609  -0.609   0.099  -0.006
   0.001   0.002   0.003   0.002   0.001
-0.020  -0.006   0.290   0.290  -0.006  -0.020
```

(c)
```
 0.481   0.512   0.572   0.572   0.512   0.481
   0.001   0.003   0.003   0.003   0.001
-0.435  -0.544  -0.829  -0.829  -0.544  -0.435
  -0.001  -0.012   0.002   0.012  -0.001
 0.454   0.458   1.583   1.583   0.458   0.454
  -0.000  -0.000           0.000   0.000
-0.454  -0.458  -1.583  -1.583  -0.458  -0.454
   0.001   0.012  -0.002   0.012   0.001
 0.435   0.544   0.829   0.829   0.544   0.435
  -0.000  -0.003  -0.003  -0.003  -0.001
-0.481  -0.512  -0.572  -0.572  -0.512  -0.481
```

(d)
```
-0.219   0.199  -0.273   0.273  -0.199   0.219
  -0.001   0.001  -0.000  -0.001   0.001
 0.199  -0.173   0.318   0.318   0.173  -0.199
   0.001   0.016  -0.000  -0.016  -0.001
-0.273   0.318   1.495   1.495  -0.318   0.273
  -0.000   0.000          -0.000   0.000
 0.273  -0.318   1.495   1.495   0.318  -0.273
  -0.001  -0.016   0.000   0.016   0.001
-0.199   0.173  -0.318   0.318  -0.173   0.199
   0.001  -0.001   0.000   0.001  -0.001
 0.219  -0.199   0.273  -0.273   0.199  -0.219
```
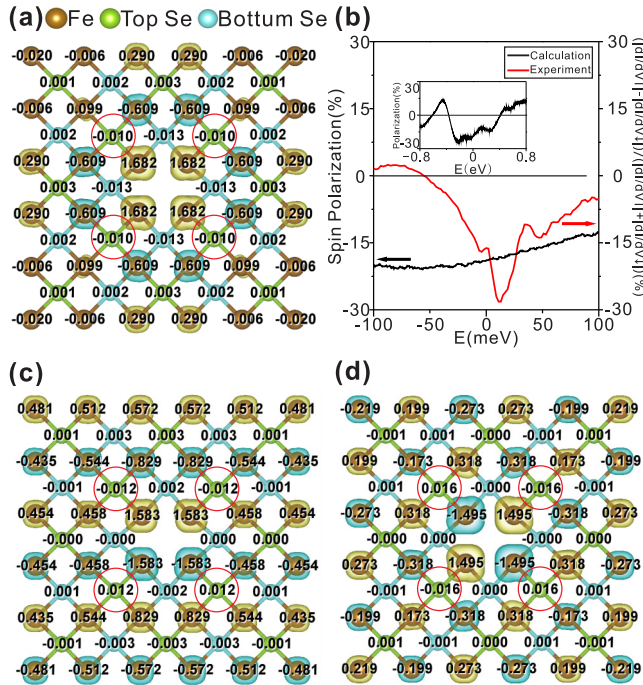
FIG. 4. The first-principle calculation of the Se vacancy in different magnetic state: The magnetic-moments distribution of FeSe thin film with a Se vacancy calculated in (a) nonmagnetic state, (c) collinear AFM order, and (d) checkerboard AFM order. The unit of numbers on top of the atoms is μ_B. The VNN Se sites measured in experiments are marked by red circles. (b) Calculated spin polarization of DOS defined as $\frac{DOS\uparrow - DOS\downarrow}{DOS\uparrow + DOS\downarrow}$ (black curves and the inset) and the spin asymmetry of the measured spin-polarized current (red curve) defined as $\frac{\frac{dI}{dV}\uparrow - \frac{dI}{dV}\downarrow}{\frac{dI}{dV}\uparrow + \frac{dI}{dV}\downarrow}$ of the VNN Se site.

in an early calculation on the FeSe system with a higher density of Se vacancies (Fe : Se = 1 : 0.875) [45]. The magnetic moments of Fe arise from the unpaired electrons due to the missing Se atom. The presence of Fe moments breaks the magnetic balance of Se atoms close to the Se vacancy. Small magnetic moments were found in the Se atoms [marked by red circles in Fig. 4(a)] closest to the Se vacancy in the top Se layer (marked by green atoms) where the spin signal was measured. Surprisingly, although the magnetic moment of Se is rather small, the spin polarization of DOS near the Fermi level is as large as -15–30% which explains the strong spin signal in the spin-polarized measurement as shown in Fig. 4(b). The seeming inconsistency between small total magnetic moments and large spin polarization near the Fermi level on Se atoms can be understood in the following way. The total magnetic moments result from the integral of spin polarization over all occupied electronic states. In the inset of Fig. 4(b), the spin polarization in large energy scale is partially positive and partially negative. Therefore, in the integral over all occupied

states, the positive spin polarization and the negative one cancel each other and finally lead to small total magnetic moments. In FeTe with bicollinear antiferromagnetic structure, SPSTM measurement also showed the spin polarization near the Fermi level as large as 60% on Te atoms [30]. The four Se atoms (marked by red circles in Fig. 4) possess the magnetic moments with the same magnitude pointing to the same direction, which agrees with the experimental measurement that fourfold symmetry is maintained. To further exclude possible AFM structure in FeSe, we calculated two AFM FeSe with a Se vacancy; one is collinear AFM [Fig. 4(c)] and the other is checkerboard AFM [Fig. 4(d)]. These AFM orders can be stabilized in the calculation, however their energies are higher by about 0.20 and 0.44 eV, respectively. In both cases, the magnetic moments on Fe atoms next to the Se vacancy are enhanced which in addition result in a small, but sizable magnetic moment on the nearest Se sites in the top Se layer as well. Nevertheless, the fourfold symmetry is broken in the four Se moments as marked by the red circle with two of them having positive value and the other two of them having negative value. This strongly opposes what we have observed in the experiment. Thus, simply from symmetry analysis, AFM orders can be ruled out in FeSe thin film.

In summary, we did SPSTM measurements on multilayer FeSe thin film grown on SrTiO$_3$(001). We found an unexpected paramagnetic signal around the Se vacancy with fourfold symmetry. Combining with the first-principle calculation, we conclude that FeSe thin film under tensile strain is nonmagnetic, even the superconductivity is suppressed, and end the controversy about the magnetic ground state in this system. Additionally, we directly show that a nominally nonmagnetic defect is able to create a cloud of local paramagnetic polarization on nearby atoms in the nonmagnetic ground state of correlated electron systems such as FeSe, which was also reported about Zn impurities in cuprate superconductors [46]. Previously, the efforts made to understand the influence of disorder and impurities in correlated electron systems mainly include NMR, superconducting quantum interference devices, muon spin rotation, and transport [47–51]. However, they measured the collective behaviors which usually make it difficult to distinguish specific defects. Here, we show that SPSTM is a powerful tool combining the fine spatial resolution with the ability of magnetic detection to measure a specific defect without perturbation from other disorders which can be directly linked to its bulk property as well.

[1] F.-C. Hsu, J.-Y. Luo, K.-W. Yeh, T.-K. Chen, T.-W. Huang, P. M. Wu, Y.-C. Lee, Y.-L. Huang, Y.-Y. Chu, D.-C. Yan *et al.*, Proc. Natl. Acad. Sci. USA **105**, 14262 (2008).

[2] X. Liu, L. Zhao, S. He, J. He, D. Liu, D. Mou, B. Shen, Y. Hu, J. Huang, and X. Zhou, J. Phys.: Condens. Matter **27**, 183201 (2015).

[3] S. Medvedev, T. McQueen, I. Troyan, T. Palasyuk, M. Eremets, R. Cava, S. Naghavi, F. Casper, V. Ksenofontov, G. Wortmann *et al.*, Nat. Mater. **8**, 630 (2009).

[4] S. Margadonna, Y. Takabayashi, Y. Ohishi, Y. Mizuguchi, Y. Takano, T. Kagayama, T. Nakagawa, M. Takata, and K. Prassides, Phys. Rev. B **80**, 064506 (2009).

[5] M. Bendele, A. Amato, K. Conder, M. Elender, H. Keller, H.-H. Klauss, H. Luetkens, E. Pomjakushina, A. Raselli, and R. Khasanov, Phys. Rev. Lett. **104**, 087003 (2010).

[6] M. Bendele, A. Ichsanow, Y. Pashkevich, L. Keller, T. Strässle, A. Gusev, E. Pomjakushina, K. Conder, R. Khasanov, and H. Keller, Phys. Rev. B **85**, 064517 (2012).

[7] W. Qing-Yan, L. Zhi, Z. Wen-Hao, Z. Zuo-Cheng, Z. Jin-Song, L. Wei, D. Hao, O. Yun-Bo, D. Peng, C. Kai *et al.*, Chin. Phys. Lett. **29**, 037402 (2012).

[8] C.-L. Song, Y.-L. Wang, Y.-P. Jiang, Z. Li, L. Wang, K. He, X. Chen, X.-C. Ma, and Q.-K. Xue, Phys. Rev. B **84**, 020503 (2011).

[9] Y. F. Nie, E. Brahimi, J. I. Budnick, W. A. Hines, M. Jain, and B. O. Wells, Appl. Phys. Lett. **94**, 242505 (2009).

[10] J.-F. Ge, Z.-L. Liu, C. Liu, C.-L. Gao, D. Qian, Q.-K. Xue, Y. Liu, and J.-F. Jia, Nat. Mater. **14**, 285 (2015).

[11] S. Tan, Y. Zhang, M. Xia, Z. Ye, F. Chen, X. Xie, R. Peng, D. Xu, Q. Fan, H. Xu *et al.*, Nat. Mater. **12**, 634 (2013).

[12] C. H. P. Wen, H. C. Xu, C. Chen, Z. C. Huang, X. Lou, Y. J. Pu, Q. Song, B. P. Xie, M. Abdel-Hafiez, D. A. Chareev, A. N. Vasiliev, R. Peng, and D. L. Feng, Nat. Commun. **7**, 10840 (2016).

[13] C.-L. Song, H.-M. Zhang, Y. Zhong, X.-P. Hu, S.-H. Ji, L. Wang, K. He, X.-C. Ma, and Q.-K. Xue, Phys. Rev. Lett. **116**, 157001 (2016).

[14] Z. R. Ye, C. F. Zhang, H. L. Ning, W. Li, L. Chen, T. Jia, M. Hashimoto, D. H. Lu, Z.-X. Shen, and Y. Zhang, arXiv:1512.02526v1 (2015).

[15] Y. Miyata, K. Nakayama, K. Sugawara, T. Sato, and T. Takahashi, Nat. Mater. **14**, 775 (2015).

[16] F. Ma, W. Ji, J. Hu, Z.-Y. Lu, and T. Xiang, Phys. Rev. Lett. **102**, 177003 (2009).

[17] F. Zheng, Z. Wang, W. Kang, and P. Zhang, Sci. Rep. **3**, 2213 (2013).

[18] H.-Y. Cao, S. Tan, H. Xiang, D. L. Feng, and X.-G. Gong, Phys. Rev. B **89**, 014501 (2014).

[19] K. Liu, Z.-Y. Lu, and T. Xiang, Phys. Rev. B **93**, 205154 (2016).

[20] K. Liu, B.-J. Zhang, and Z.-Y. Lu, Phys. Rev. B **91**, 045107 (2015).

[21] M. Hirayama, T. Misawa, T. Miyake, and M. Imada, J. Phys. Soc. Jpn. **84**, 093703 (2015).

[22] R. Yu and Q. Si, Phys. Rev. Lett. **115**, 116401 (2015).

[23] A. V. Chubukov, R. M. Fernandes, and J. Schmalian, Phys. Rev. B **91**, 201105 (2015).

[24] A. Kreisel, S. Mukherjee, P. J. Hirschfeld, and B. M. Andersen, Phys. Rev. B **92**, 224515 (2015).

[25] T. Shimojima, Y. Suzuki, T. Sonobe, A. Nakamura, M. Sakano, J. Omachi, K. Yoshioka, M. Kuwata-Gonokami, K. Ono, H. Kumigashira *et al.*, Phys. Rev. B **90**, 121111 (2014).

[26] M. Watson, T. Kim, A. Haghighirad, N. Davies, A. McCollam, A. Narayanan, S. Blake, Y. Chen, S. Ghannadzadeh, A. Schofield *et al.*, Phys. Rev. B **91**, 155106 (2015).

[27] P. Zhang, T. Qian, P. Richard, X. Wang, H. Miao, B. Lv, B. Fu, T. Wolf, C. Meingast, X. Wu *et al.*, Phys. Rev. B **91**, 214503 (2015).

[28] J. Maletz, V. Zabolotnyy, D. Evtushinsky, S. Thirupathaiah, A. Wolter, L. Harnagea, A. Yaresko, A. Vasiliev, D. Chareev, A. Böhmer *et al.*, Phys. Rev. B **89**, 220506 (2014).

[29] Y. Zhou, L. Miao, P. Wang, F. F. Zhu, W. X. Jiang, S. W. Jiang, Y. Zhang, H. F. Ding, H. Zheng, J. F. Jia, D. Qian, and D. Wu, arXiv:1611.03603v2 (2017).

[30] M. Enayat, Z. Sun, U. R. Singh, R. Aluru, S. Schmaus, A. Yaresko, Y. Liu, C. Lin, V. Tsurkan, A. Loidl *et al.*, Science **345**, 653 (2014).

[31] R. Wiesendanger, Rev. Mod. Phys. **81**, 1495 (2009).

[32] P. Hohenberg and W. Kohn, Phys. Rev. **136**, B864 (1964).

[33] P. E. Blöchl, Phys. Rev. B **50**, 17953 (1994).

[34] G. Kresse and J. Furthmüller, Comput. Mater. Sci. **6**, 15 (1996).

[35] G. Kresse and J. Furthmüller, Phys. Rev. B **54**, 11169 (1996).

[36] D. M. Ceperley and B. J. Alder, Phys. Rev. Lett. **45**, 566 (1980).

[37] J. P. Perdew, K. Burke, and M. Ernzerhof, Phys. Rev. Lett. **77**, 3865 (1996).

[38] Z. Li, J.-P. Peng, H.-M. Zhang, W.-H. Zhang, H. Ding, P. Deng, K. Chang, C.-L. Song, S.-H. Ji, L. Wang *et al.*, J. Phys.: Condens. Matter **26**, 265002 (2014).

[39] D. Huang, T. A. Webb, C.-L. Song, C.-Z. Chang, J. S. Moodera, E. Kaxiras, and J. E. Hoffman, Nano Lett. **16**, 4224 (2016).

[40] Y. Fang, D. H. Xie, W. Zhang, F. Chen, W. Feng, B. P. Xie, D. L. Feng, X. C. Lai, and S. Y. Tan, Phys. Rev. B **93**, 184503 (2016).

[41] C.-L. Song, Y.-L. Wang, P. Cheng, Y.-P. Jiang, W. Li, T. Zhang, Z. Li, K. He, L. Wang, J.-F. Jia *et al.*, Science **332**, 1410 (2011).

[42] Z. Wang, H. Zhang, D. Liu, C. Liu, C. Tang, C. Song, Y. Zhong, J. Peng, F. Li, C. Nie *et al.*, Nat. Mater. **15**, 968 (2016).

[43] I. I. Mazin, M. D. Johannes, L. Boeri, K. Koepernik, and D. J. Singh, Phys. Rev. B **78**, 085104 (2008).

[44] D. J. Singh, Phys. C (Amsterdam, Neth.) **469**, 418 (2009).

[45] K.-W. Lee, V. Pardo, and W. E. Pickett, Phys. Rev. B **78**, 174502 (2008).

[46] H. Alloul, J. Bobroff, M. Gabay, and P. Hirschfeld, Rev. Mod. Phys. **81**, 45 (2009).

[47] J. Chakhalian, R. Kiefl, R. Miller, J. Brewer, S. Dunsiger, G. Morris, W. MacFarlane, J. Sonier, S. Eggert, I. Affleck *et al.*, Phys. Rev. Lett. **91**, 027202 (2003).

[48] H. Alloul, P. Mendels, H. Casalta, J. F. Marucco, and J. Arabski, Phys. Rev. Lett. **67**, 3140 (1991).

[49] S. Zagoulaev, P. Monod, and J. Jegoudez, Phys. Rev. B **52**, 10474 (1995).

[50] C. Tarantini, M. Putti, A. Gurevich, Y. Shen, R. Singh, J. Rowell, N. Newman, D. Larbalestier, P. Cheng, Y. Jia *et al.*, Phys. Rev. Lett. **104**, 087002 (2010).

[51] S. Teknowijoyo, K. Cho, M. Tanatar, J. Gonzales, A. Böhmer, O. Cavani, V. Mishra, P. Hirschfeld, S. Bud'ko, P. Canfield *et al.*, Phys. Rev. B **94**, 064521 (2016).